Applied Catalysis B: Environmental 205 (2017) 368–375

Contents lists available at ScienceDirect

Applied Catalysis B: Environmental

journal homepage: www.elsevier.com/locate/apcatb

In situ surface assembly of core-shell TiO_2-copper(I) cluster nanocomposites for visible-light photocatalytic reduction of Cr(VI)☆

Wei Ji[a], Jian Qu[a,b], Cheng-An Li[a], Jing-Wei Wu[a], Su Jing[a,*], Fei Gao[c], Yi-Nong Lv[d], Chang Liu[d], Dun-Ru Zhu[d], Xiao-Min Ren[a], Wei Huang[b]

[a] School of Chemistry and Molecular Engineering, Nanjing Tech University, Nanjing 211816, PR China
[b] Institute of Advanced Materials, Nanjing Tech University, Nanjing 210009, PR China
[c] Jiangsu Key Laboratory of Vehicle Emissions Control Center of Modern Analysis, Nanjing University, Nanjing 210093, PR China
[d] School of Chemistry and Chemical Engineering, Nanjing Tech University, Nanjing 210009, PR China

ARTICLE INFO

Article history:
Received 29 October 2016
Received in revised form
11 December 2016
Accepted 17 December 2016
Available online 19 December 2016

Keywords:
Polymeric $[Cu_2I_2\mathbf{L}_2]_n$ cluster
Selenoanthracene
TiO_2
Charge-transfer complex
Visible-light photocatalyst

ABSTRACT

1D loop chain copper(I) cluster, $[Cu_2I_2\mathbf{L}_2]_n$, can be obtained based upon 9-(3-phenylselanyl-2-phenylselanylmethylpropyl)anthracene (**L**) and CuI. A facile *in situ* surface assembly strategy was designed to construct polymeric $[Cu_2I_2\mathbf{L}_2]_n$ on the surface of TiO_2 nanoparticles. The visible-light photocatalytic property of core-shell TiO_2-$[Cu_2I_2\mathbf{L}_2]_n$ was confirmed by effective reduction of aqueous chromium(VI), showing a clear correlation to optical absorption (Eg = 2.8 eV). The key points of this strategy include high reactivity between copper(I) and soft selenium atom, efficient charge-transfer through polymeric cluster shell, and visible-light photoactivity of copper(I) halogen clusters.

© 2016 Elsevier B.V. All rights reserved.

1. Introduction

Water pollution is one of the top ten problems that humanity is facing in the 21 st century. The key issue for the treatment and reuse of wastewater is the effective removal of hazardous contaminants. As one of the most toxic and important heavy metals, chromium(VI) causes severe health threats to human beings. The photocatalytic reduction of chromium(VI) into non-toxic chromium(III) using photogenerated electrons from TiO_2 has been confirmed to be economic and environmentally friendly method [1–4]. To take advantage of the visible solar spectrum, there are two most efficient strategies to narrow the band gap of TiO_2 [5]. The first is doping or co-doping, which refers to the substitution of non-metal (B, C, and N) or metal (Fe, Co, Ni and Cr) at Ti^{4+} and O^{2-} sites [6–8]. The other and more convenient way is sensitization by absorbing dyes, the photochemical process of which can be initiated by the visible-light photoexcitation of dye, followed by electron transfer from the excited state dye to TiO_2 conduction band [9–12]. Up to now, the highest conversion efficient sensitizers reported are Ru(II)-pyridine and its substituted derivatives, with relatively high absorption coefficients in the visible region, long-lived excited states, and chemical stability [9,13]. However, the drawbacks of such Ru(II)-sensitizers are the high-cost and low natural abundance. Copper(I) complexes can display longer excited state lifetimes due to their d^{10} configuration, which in principle exhibit similar electronic transition energies and photophysical properties as some of the Ru(II) complexes [14–21]. Moreover, copper(I) complexes are environmentally friendly and economically available. Sauvage et al. [14] demonstrated the potential of copper(I) sensitizers with colloidal films of ZnO and TiO_2 as substrates. Chen found that it can be prevented by constraining the copper(I) metal center within a rigid environment by employing bulky ligands or adding aryl groups to flatten the pseudo-tetrahedral ground state geometry and provide longer wavelength absorption for light harvesting [17,19,22]. The team of Constable and Housecroft performed 'surfaces-as-ligands, surfaces-as-complexes' approach to construct heteroleptic copper(I) sensitizers on the surface of TiO_2, which was proved to be atom-efficient strategy [23–26]. Although a variety of copper(I) complexes sensitization have been investigated, we can find that all of them exist as discrete molecules on TiO_2 surface, and are based on ligands bearing hard donor atoms like N. These limit the stability and optical efficiency of the copper compounds in photovoltaic

☆ CCDC numbers 1469260 and 1469261. For crystallographic data in CIF or other electronic format see Supplementary materials.

* Corresponding author.
E-mail address: sjing@njtech.edu.cn (S. Jing).

http://dx.doi.org/10.1016/j.apcatb.2016.12.041
0926-3373/© 2016 Elsevier B.V. All rights reserved.

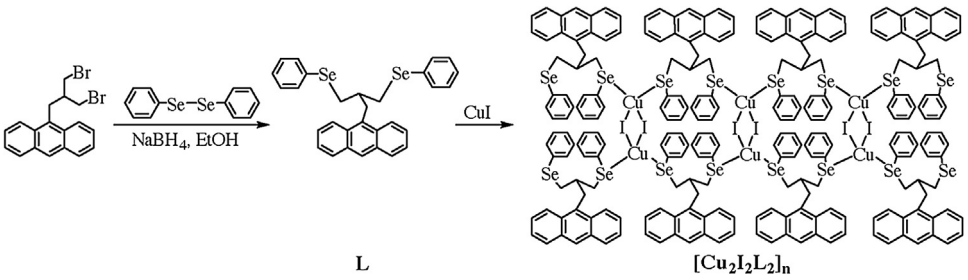

Scheme 1. Synthetic routes for **L** and $[Cu_2I_2\mathbf{L}_2]_n$.

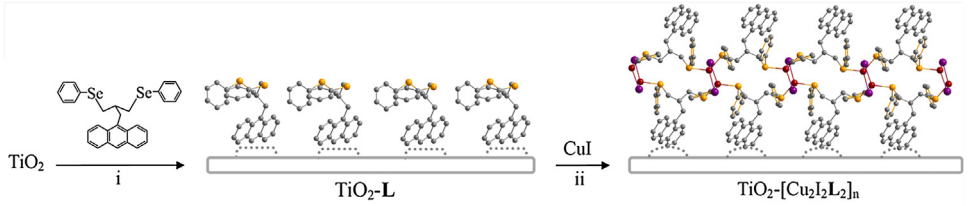

Scheme 2. *In situ* preparation of core-shell TiO_2-$[Cu_2I_2\mathbf{L}_2]_n$.

applications. In this regard, it is highly demanded to design novel copper(I) sensitizers to overcome the above limitations.

As one important branch of copper(I) complexes, copper(I) cluster with formula $Cu_xX_yL_z$, where X = Cl, Br or I and L = ligand, have attracted considerable attention due to their diverse multidimensional structures and potential applications in luminescence material [27–30], molecular sensor[31,32] and catalyst in C—N coupling reactions [33]. Li et al. demonstrated the potential of Cu_2I_2/metallosalen coordination polymers in the photodegradation of MB under visible-light illumination. The synergetic effect of Cu_2I_2 cluster and metallosalen may show the existence of the electron transfer pathways between them [34,35]. Combining the stable tetrahedral coordination sphere of optical activity copper(I) and the halide donor, there exists the possibility to construct multidimensional copper(I) cluster out of nano TiO_2 core, which may lead to higher stability, and efficient photo-induced charge transportation and separation [36–39]. To our best knowledge, there is still no report of polymeric copper(I) cluster sensitized TiO_2 and the related photocatalytic study.

Soft Se donor atoms can form stable copper(I) complexes than N, P and O, our continued interest in the coordination chemistry of selenoethers led us to investigate the synthesis and characterization of new neutral selenoethers copper(I) cluster and explore their catalytic activity [33,40]. In light of stable charge-transfer complexes formed between TiO_2 and polycyclic aromatic compound through physical adsorption [12,41,42], a bidentate selenoether ligand containing one anthrancene unit, 9-(3-phenylselanyl-2-phenylselanylmethylpropyl)anthracene (**L**), was designed and synthesized (Scheme 1). Studies show that **L** can easily form polymeric copper(I) iodide cluster $[Cu_2I_2\mathbf{L}_2]_n$. Herein, an *in situ* assembly method was designed to construct polymeric cluster on TiO_2 surface, giving TiO_2-$[Cu_2I_2\mathbf{L}_2]_n$ nanocomposites. (Scheme 2) [43]. The investigation addresses the photocatalytic property of TiO_2-$[Cu_2I_2\mathbf{L}_2]_n$ taking Cr(VI) as a probe under visible-light illumination.

2. Materials and methods

2.1. Reagents

Diphenyl diselenide, sodium boron hydride, 1,5-diphenyl carbazide, potassium dichromate ($K_2Cr_2O_7$), Cu(I) halides and TiO_2 (Degussa P25, 75% anatase, 25% rutile, size:~25 nm) were purchased from commercial suppliers and used without other purification prior to use. All used chemicals were of AR grade. Acetonitrile, ethanol, dichloromethane, tetrahydrofuran, ethyl acetate, N,N-dimethylformamide, *n*-hexane and petroleum ether used for syntheses were purified and dried following standard procedures prior to use. Experimental temperatures in the product formation studies and photocatalytic research were maintained using either a thermostatted refrigerated recirculating bath or thermostatted heated oil bath. The synthetic of ligands manipulations were performed in Schlenk Line. Deionized water was used throughout the experiments.

2.2. Characterization

^{1}H NMR spectra were recorded at ambient temperature on a Bruker DRX spectrometer (300 MHz) and its chemical shifts were referenced to the solvent signal in $CDCl_3$. Electrospray ionization mass spectra (ESI–MS) were recorded with a Finnigan mat APISSQ 710 mass spectrometer, *m*/*z* values have been rounded to the nearest integer or half-integer; assignments are based on isotopomers containing ^{1}H, ^{12}C, and ^{80}Se; expected isotope distribution patterns were observed. Elemental analyses of C, H were performed on a Perkin-Elmer 2400 CHO elemental analyzer. Melting points were determined using the cover glass and uncorrected.

High Resolution transmission electron microscopy (HR-TEM) analyses were accomplished by JEOL JEM-2100F Field Emission Electron Microscope. X-ray photoelectron spectroscopy (XPS) with PHI 5000 VersaProbe of UlVAC-PHI and all binding energies were referenced to the C1 s peak at 284.8 eV. Fourier transform infrared spectroscopy (FTIR) was recorded within the 400–4000 cm^{-1} region on a Thermo Scientific Nicolet IS10 FTIR spectrometer using KBr pellets. UV–vis diffuse reflectance spectra (UV–vis DRS) were recorded using PerkinElmer Lambda 950 UV/Vis/NIR Spectrophotometer, with $BaSO_4$ as the reference. Electrochemical measurements were performed at room temperature in a dry MeCN containing a 0.1 M [*n*-NBu_4][PF_6] electrolyte using a CHI 660D electrochemical workstation of Shanghai CH Instruments Co. The sweep rate for cyclic voltammetry was 100 mV s^{-1}. A three electrode arrangement was used with a Pt working electrode modified with $[Cu_2I_2\mathbf{L}_2]_n$ film, a Pt wire counter electrode, and an Ag/Ag^+ (0.01 M $AgNO_3$ in MeCN) reference electrode. The sweep

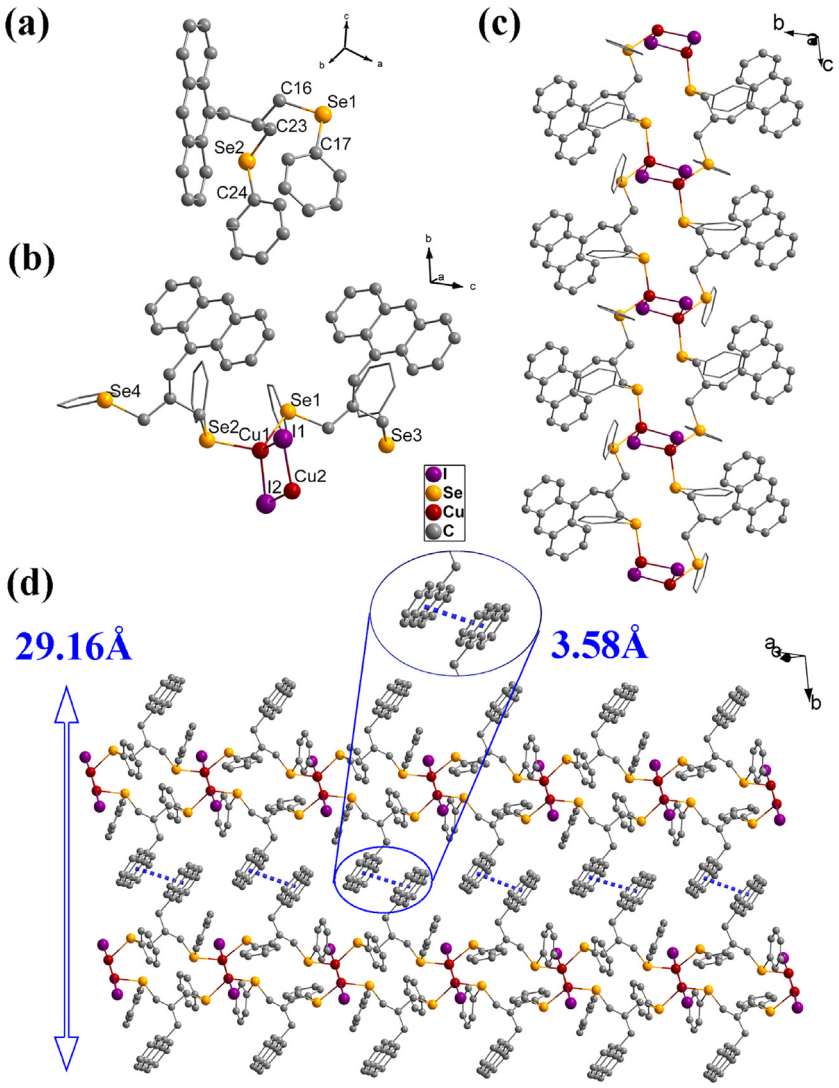

Fig. 1. (a) View of molecular structure of **L**; (b) The asymmetric unit of $[Cu_2I_2\mathbf{L}_2]_n$; (c) View of 1D loop chain in $[Cu_2I_2\mathbf{L}_2]_n$; (d) View of packing diagram along the *b* axis in $[Cu_2I_2\mathbf{L}_2]_n$. Hydrogen atoms have been omitted for clarity.

rate for cyclic voltammetry was 100 mV s^{-1}. The modified working electrode was prepared through dropping the solution of ultrasonically dissolving 0.05 M $[Cu_2I_2\mathbf{L}_2]_n$ in DMF on the electrode surface for three times, and then dried at 30 °C under vacuum. UV–vis absorption spectra were measured with HITACHI spectrophotometer UV-3900.

All single-crystal X-ray diffraction measurements were performed using a Bruker SMART APEX II CCD diffractometer with graphite monochromated Mo K_α radiation (λ = 0.71073 Å) and a rotating anode generator at ambient temperature (293–296 K). Each suitable size single crystal was mounted on glass capillary using protecting oil. A hemisphere of data was collected using a narrow-frame method with scan widths of 0.30°in ω and an exposure time of 10 s per frame. Data were integrated using the Siemens SAINT program, with intensities corrected for Lorentz factor, polarization, air absorption, and absorption due to variation in the path length through the detector faceplate. Multi-scan absorption corrections were applied. The structures were solved by direct methods and refined on F^2 least-squares method using SHELXL-2014 [44]. Non-hydrogen atoms were refined anisotropically, and hydrogen atoms were geometrically fixed with displacement parameters equivalent to 1.2 times that of the atoms to which they were bonded.

2.3. Synthesis of **L** and $[Cu_2I_2\mathbf{L}_2]_n$

L: 0.156 g (0.5 mmol) diphenyl diselenide was dissolved in C_2H_5OH in N_2 atmosphere, ice bath for 5 mins, 0.767 g $NaBH_4$ was added to the flask and continue to ice bath for 15 min. Then the reaction was kept at room temperature for 2 h 9-(3′-bromo-2′-bromomethylpropyl)anthracene 0.098 g (0.25 mmol) was added, and the mixture left to stir for 5 h at room temperature. The solvent was removed by evaporation under reduced pressure. The residue was treated with H_2O (50 mL) and then extracted with CH_2Cl_2 (3 × 50 mL). The extract was dried over $MgSO_4$, evaporated to dryness, then subjected to column chromatography on SiO_2. The target product, an orange solid (0.049 g, 43%), was obtained by elution with *n*-C_6H_{14}/CH_2Cl_2 (5:1). Single crystals of **L** was obtained by slow evaporation of a mixed solution *n*-C_6H_{14}/CH_2Cl_2 (1:1), which afforded yellow lamellar crystal suitable for single crystal X-ray diffraction. ^{1}H NMR (400 MHz, $CDCl_3$) (δ, ppm): 8.38 ($C_{14}H_9$, H_{10}, s.1H), 8.21 ($C_{14}H_9$, H_{1+8}, d, 2H), 8.00 ($C_{14}H_9$, H_{4+5}, d, 2H), 7.46 – 7.35 ($C_{14}H_9$, m, 4H), 7.13(C_6H_5, d, 4H), 7.06 (C_6H_5, d, 2H), 6.98 (C_6H_5, t, 4H), 3.87 ($ArCH_2C$, d, 2H), 3.18 (CCH_2 Se, m, 2H), 2.99 (CCH_2 Se, m, 2H), 2.54 (CCHCSe, m, 1H). ES MS: 562.03 ($[M+1]^+$). Elemental analysis calcd (%): C 66.18, H 4.81; found: C 66.17, H 4.83. M.p.

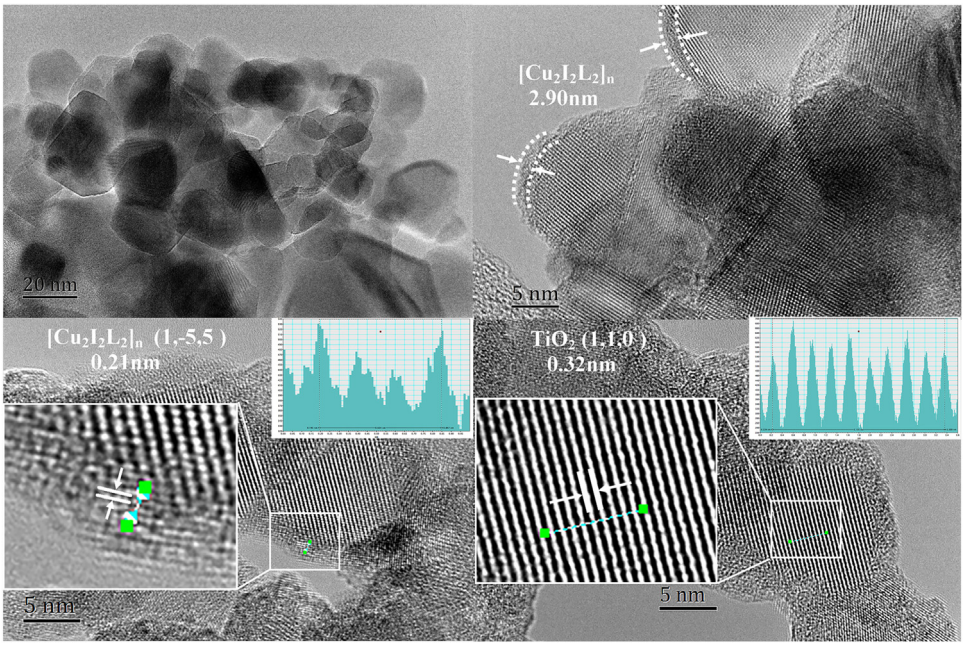

Fig. 2. HR-TEM micrographs of TiO_2-$[Cu_2I_2\mathbf{L}_2]_n$.

217–218 °C. UV–vis, λ_{max}/nm (1×10^{-5} M CH_2Cl_2, $\varepsilon_{max}/M^{-1}\,cm^{-1}$): 372 ($6.8 \times 10^4$). FTIR (solid, ν, cm^{-1}): 3049, 1558, 1541, 1507, 1479.

$[Cu_2I_2\mathbf{L}_2]_n$: The MeCN solution of CuI (0.005 g, 0.025 mmol) was added slowly to CH_2Cl_2 solution of **L** (0.014 g, 0.025 mmol) with the 1:1 molar ratio. Note that the reaction of metal salts with ligands did yield the suitable single crystals of the desired new products just through facile interface diffusion. The yellow needle crystals can be easily separated through the microscope, yield 7.57 mg, 41.2%. Elemental analysis calcd (%) of $[Cu_2I_2\mathbf{L}_2]_n$ ($C_{60}H_{52}Cu_2I_2Se_4$): C 49.03, H 3.57; found: C 49.06, H 3.55. M.p. 273–274 °C. FTIR (solid, ν, cm^{-1}): 3050, 2965, 1580, 1518, 1435, 1350.

2.4. Preparation of TiO_2-$[Cu_2I_2\mathbf{L}_2]_n$ nanocomposites

0.544 g (1 mmol) of **L** was added in 40 mL MeCN and produced a yellow solution under magnetic stirring. Then 0.080 g (1 mmol) of TiO_2 was dispersed into the above suspension ultrasonic for 30 min. The mixture was stirred at room temperature in the dark for 24 h. After centrifugation, the formed pale yellow nanoparticles were moved into 40 mL MeCN solution of CuI (0.190g, 1 mmol) and then stirred for a further 24 h. The yellow suspension was centrifugal separated. Repeat the previous impregnation (ligand solution and metal solution). The sensitized TiO_2 was washed with MeCN for three times to eliminate the deposition of uncoordinated **L** and CuI on the TiO_2 surface. The final product was dried at 60 °C under vacuum.

2.5. Evaluation of visible-light catalytic activity

10 mg TiO_2-$[Cu_2I_2\mathbf{L}_2]_n$ were mixed with 30 mL 1×10^{-4} M $K_2Cr_2O_7$ aqueous solution in a glass tube with a volume of 50 mL. H_2SO_4 were used to adjust aqueous solution pH to 2.

All photoreactions were done after 30 min of adsorption-desorption equilibrium. For the photo-catalytic activity tests, a 300 W metal halide lamp (HL) that emits both UV and visible-light over a wide wavelength was employed as a light source. Light was filtered through a 1 M $NaNO_2$ solution to cut off wavelengths shorter than 400 nm and then focused onto a 50 mL glass tube reactor. The light intensity was ca. 300 mW/cm^2 measured by a Digital Lux Meter TES 1332A. During the reaction, the reactor was stirred magnetically and injected with air by a pump. Sample aliquots were withdrawn from the reactor intermittently and centrifuged with 10000 r/min for 1 h, the liquid for UV analytical testing and precipitate for recycling experiment.

Photoreduction of Cr(VI) to Cr(III) was analyzed using a colorimetric method that uses 1,5-diphenylcarbizide (DPC) reagent. The color change at 540 nm was monitored using a UV–vis spectrophotometer [3].

3. Results and discussion

3.1. Synthesis and crystallographic studies of **L** and $[Cu_2I_2\mathbf{L}_2]_n$

L and $[Cu_2I_2\mathbf{L}_2]_n$ were synthesized similarly via a method described by us previously, as shown in Scheme 1 [40]. And they have been fully characterized by analytical and spectroscopic means (see Experimental and ESI). X-ray crystallographic studies show that, **L** crystallize in the monoclinic $P2_1/n$ and $[Cu_2I_2\mathbf{L}_2]_n$ in the triclinic $P\bar{1}$ space group, respectively. As shown in Fig. 1, the asymmetric unit of $[Cu_2I_2\mathbf{L}_2]_n$ contains two **L**, two crystallographically independent Cu(I) ions, two μ_2-I counterions. Both Cu(I) ions display a distorted tetrahedral geometry comprising two μ_2-I ions and two Se atoms from two different ligands. The bond lengths and angles around Cu(I) are similar to the values found in the rhomboid Cu_2I_2 unit [33,40]. Two μ_2-I ions are bound to two symmetry-related Cu(I) ions forming a Cu_2I_2 rhomboid dimer, in which Cu(I) ions are separated by distances of 2.681(3) Å which is slightly shorter than those in the 1D chain Cu_2I_2 dimer reported by us previously (2.804-2.807 Å) [33]. Each **L** connects two independent Cu_2I_2 units together giving rise to a 1D loop chain along *c* axis. The crystal packing diagram of $[Cu_2I_2\mathbf{L}_2]_n$ in Fig. 1d show that the centroid-to-centroid distance and tilt angle between anthracene rings from different chains are 3.582 Å and 1.305°, respectively. These shows the presence of a strong face-to-face π-π stacking interaction which not only tune absorption property, lead to increased lifetimes of excited states, but also can promote effective electrons transfer between 1D chains [45,46]. Crystallographic

Table 1
Crystal data and refinement details for **L** and $[Cu_2I_2\mathbf{L}_2]_n$.

	L	$[Cu_2I_2\mathbf{L}_2]_n$
Empirical formula	$C_{30}H_{26}Se_2$	$C_{60}H_{52}Cu_2I_2Se_4$
Formula weight	544.43	1469.73
Crystal system	Monoclinic	Triclinic
Space group	$P2_1/n$	P-1
T (K)	296(2)	293(2)
wavelength/Å	0.71073	0.71073
$a/b/c$ Å	15.6268(13)/9.4662(8)/16.5372(14)	12.716(4)/14.033(4)/15.459(4)
$\alpha/\beta/\gamma$ deg	90.00/98.030(2)/90.00	96.247(3)/102.734(3)/93.490(3)
V/Å^3	2422.3(4)	2664.5(13)
Z	4	2
D_{calcd}/Mg·m^{-3}	1.493	1.832
μ/mm^{-1}	3.068	4.728
F(000)	1096	1424
Reflections/Unique	17061/5999	18892/9289
Parameters/Restraints	289/1	615/0
θ range/deg	1.933–28.293	1.361–25.005
R_{int}	0.0233	0.0380
R_1 [$I>2\sigma(I)$]wR_2 [$I>2\sigma(I)$]	0.0337	0.0379
	0.0746	0.0939
GOF Residuals/e·Å^{-3}	1.012	0.996
	0.236/−0.512	0.698/−1.232

data, structure refinement details of **L** and $[Cu_2I_2\mathbf{L}_2]_n$ are presented in Table 1.

3.2. In situ *self-assembly of TiO_2-$[Cu_2I_2\mathbf{L}_2]_n$ nanocomposites*

Inspiring from the success of 'surfaces-as-ligands, surfaces-as-complexes' approach, an *in situ* self-assembly method of $[Cu_2I_2\mathbf{L}_2]_n$ directly on the TiO_2 surface was designed as shown in Scheme 2 (for more details see Experimental). TiO_2 nanoparticles were first immersed into a MeCN solution of **L** for 24 h. The pale yellow nanoparticles were centrifuged and then immersed into a MeCN solution of CuI for 24 h. Repeat the previous impregnation again in **L** solution and CuI solution sequentially. After washing with MeCN and drying, the nanoparticles retained a yellow color, the color change is indicative of coordination occurring on the surface of TiO_2.

The morphology of TiO_2-$[Cu_2I_2\mathbf{L}_2]_n$ was investigated by the high resolution transmission electron microscopy (HR-TEM), shown in Fig. 2. There exhibited well-defined lattice fringes in both substrate TiO_2 and sensitizer $[Cu_2I_2\mathbf{L}_2]_n$, where the lattice spacing was estimated to be ca. 0.32 nm and 0.21 nm. These are equal to the lattice parameter in the (110) facet of anatase TiO_2 and the (155) facet of $[Cu_2I_2\mathbf{L}_2]_n$. A layer of sensitizer with approximate 2.90 nm thickness is coated on TiO_2 surface, which is in agree with the thickness of two 1D chains with face-to-face π-π stacking interaction in $[Cu_2I_2\mathbf{L}_2]_n$ (2.91 nm, obtained from crystallographic study, Fig. 1d), suggesting the successful preparation of core-shell nanoparticles [47–49].

X-ray photoelectron spectra (XPS) further confirmed the successful assembly of $[Cu_2I_2\mathbf{L}_2]_n$ on the surface of the TiO_2 and the elemental compositions of sample (Fig. 3). The binding energies for Cu2p and I3d in TiO_2-$[Cu_2I_2\mathbf{L}_2]_n$, 931.5/951.5 eV and 618.8/630.3 eV, are consistent with those reported in literatures [50,51]. The C1s spectrum of TiO_2-$[Cu_2I_2\mathbf{L}_2]_n$, in Fig. 3c, can be separated into two peaks, 284.8 and 291.1 eV, the latter is indicative of the aromatic organic compounds on the TiO_2 surface and is tentatively assigned to low-energy π-π* transitions [52–54]. In addition, for bare TiO_2, the O1s peaks consisted of a dominant peak at 529.9 eV and another higher energy peak at 532.5 eV, which can be indexed to Ti—O bonding and O—H bonding coming from the water molecule adsorbed on the surface of TiO_2. Compared with the O1s XPS analysis of TiO_2-$[Cu_2I_2\mathbf{L}_2]_n$/TiO_2-**L** (Fig. 3d), the ratio of higher peak and lower peak has been obviously changed, which can be attributed to the formation of charge-transfer complex between $[Cu_2I_2\mathbf{L}_2]_n$ and TiO_2 [55].

Fourier-transform infrared (FTIR) spectroscopy also confirmed the sensitization of $[Cu_2I_2\mathbf{L}_2]_n$ on the TiO_2 surface. The spectrum of TiO_2-$[Cu_2I_2\mathbf{L}_2]_n$ displays characteristics bands centered at 2959, 2922, 1540, 1515, 1456, 1382 cm^{-1} which can be assigned to the bending modes of C—H and C=C vibration of aromatic units (Fig. S4) [56]. The powder XRD pattern of TiO_2-$[Cu_2I_2\mathbf{L}_2]_n$ shows no additional peaks or shifts in the existing peaks of TiO_2 (Fig. S6) [57].

As shown in Fig. 4a, the UV–vis DR spectra clearly support the sensitization of TiO_2 by $[Cu_2I_2\mathbf{L}_2]_n$. The most significant band of cluster $[Cu_2I_2\mathbf{L}_2]_n$ shows broad and strong visible absorption centered at 414 nm which can be ascribed to visible-light response of copper(I)-based solids [35]. Compared to TiO_2, TiO_2-$[Cu_2I_2\mathbf{L}_2]_n$ shows red shift in the absorption edge, 408 nm, which can be attributed to the charge-transfer complex formed between TiO_2 and $[Cu_2I_2\mathbf{L}_2]_n$. The Tauc plot of TiO_2-$[Cu_2I_2\mathbf{L}_2]_n$ gives that the energy of absorption band edge is 2.8 eV, a significant decrease with respect to that observed for free TiO_2 (3.2 eV) [58]. The corresponding band gap lies now in the visible region (Fig. 4b), which suggests that TiO_2-$[Cu_2I_2\mathbf{L}_2]_n$ is potential candidate to drive the photocatalytic reaction under visible-light irradiation as compared to bare TiO_2.

The cyclic voltammetry (CV) of $[Cu_2I_2\mathbf{L}_2]_n$ shows one quasi-reversible redox wave with the ground state oxidation potential E_{ox} at 1.278 V (Fig. S7). From the absorption onset λ_{onset} = 320 nm in Fig. 4, the zero–zero excitation energy E_{0-0} is estimated to be 3.875 eV ($E_{0-0} = 1240/\lambda_{onset}$). The excited state oxidation potential E^*_{ox} is then calculated by $E^*_{ox} = E_{ox} - E_{0-0} = -2.597$ V [58,59]. It has been highlighted that the sensitizer excited state needs to be sufficiently high in energy to allow high electron transfer efficiencies. So, the deduced E^*_{ox} of $[Cu_2I_2\mathbf{L}_2]_n$ are more negative than the conduction band edge of TiO_2 (−0.5 V vs. NHE) [60], indicating that the electron transfer process is energetically favorable.

3.3. *Photocatalytic activity*

The photocatalytic reduction of aqueous Cr(VI) was carried out to evaluate the photoreduction ability of catalyst. As shown in Fig. 5a, only TiO_2-$[Cu_2I_2\mathbf{L}_2]_n$ exhibits good photoreduction activity to Cr(VI), the concentration of Cr(VI) decreased to almost zero within 120 min of visible-light irradiation (λ > 400 nm). It's noteworthy that there is no photoactivity of TiO_2 and free $[Cu_2I_2\mathbf{L}_2]_n$

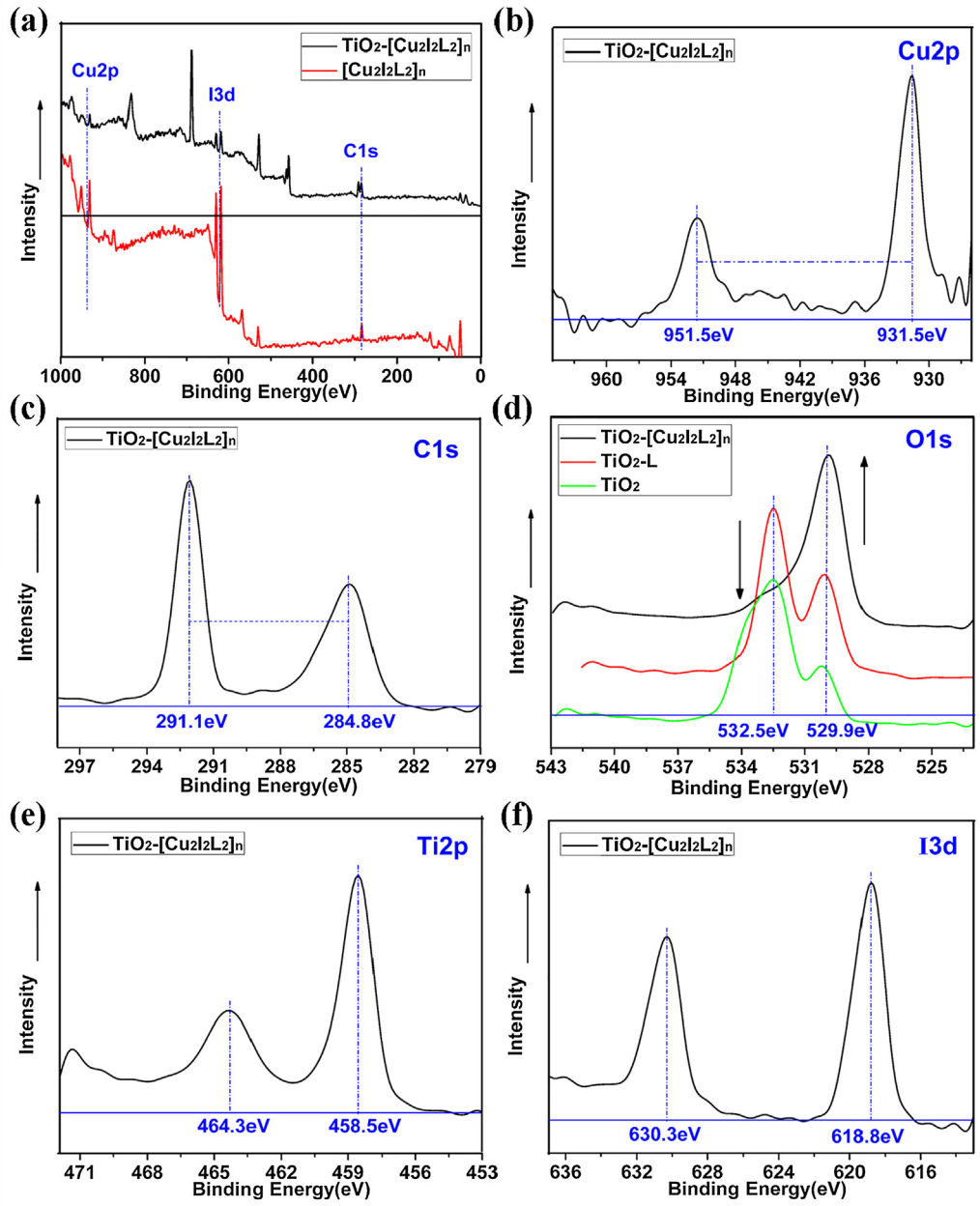

Fig. 3. XPS spectra of TiO_2-$[Cu_2I_2\mathbf{L}_2]_n$ and $[Cu_2I_2\mathbf{L}_2]_n$ (a), high-resolution Cu2p (b), C1s (c), Ti2p (e) and I3d (f), O1s in TiO_2-$[Cu_2I_2\mathbf{L}_2]_n$/TiO_2-**L**/TiO_2 (d).

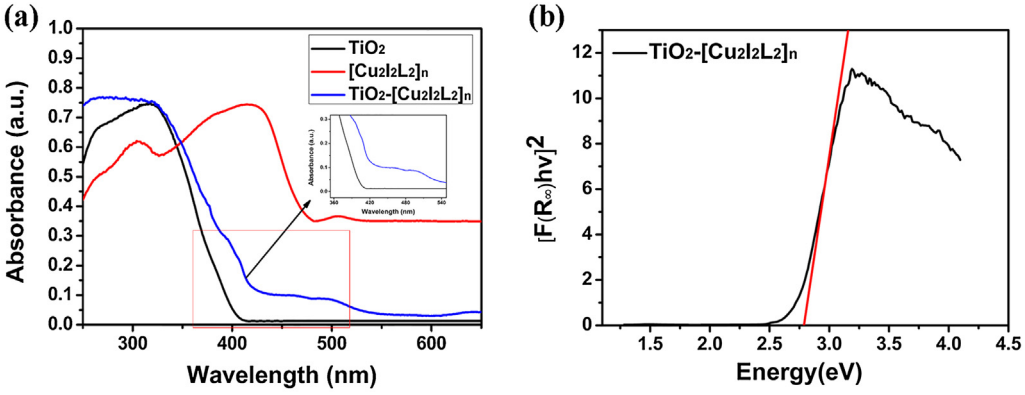

Fig. 4. UV–vis DRS and the band gap estimation of TiO_2-$[Cu_2I_2\mathbf{L}_2]_n$ using a Tauc plot.

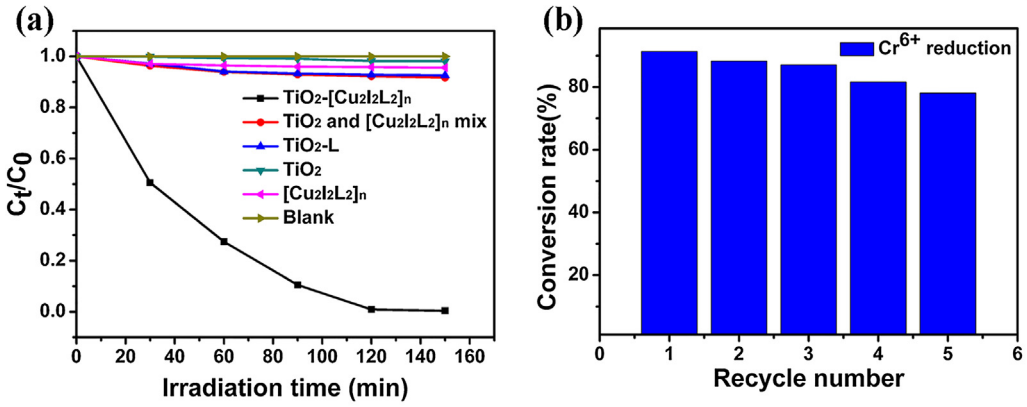

Fig. 5. (a) Photoreduction aqueous Cr(VI) under visible-light (λ > 400 nm) with 20 mg different catalysts and blank. (C_0: Initial Cr(VI) concentrations; C_t: Cr(VI) concentrations after irradiation.); (b) Photoreduction aqueous Cr(VI) conversion rate with TiO_2-$[Cu_2I_2\mathbf{L}_2]_n$ reused time.

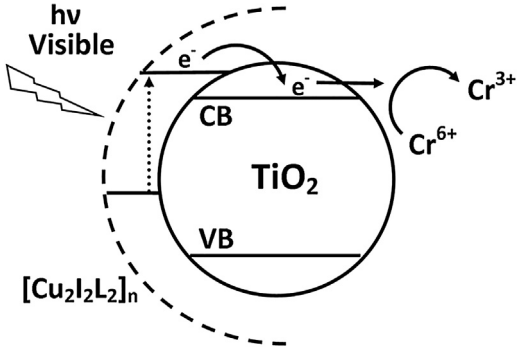

Fig. 6. Outline of a possible pathway for photoreduction of Cr(VI).

mixture, which means that the formation of effective charge-transfer complex is important for the photogenerated electrons transfer.

The stability and recoverability are essential for the practical application of photocatalysis. The recycling runs of the TiO_2-$[Cu_2I_2\mathbf{L}_2]_n$ nanocomposites in removing Cr(VI) was evaluated, as shown in Fig. 5b. Each cycle run is followed by another cycle run without any elution or desorption. After repeating the photoreduction of Cr(VI) for five times, the efficiency of reduction still keep at 78.1%. The XPS and FTIR spectra of TiO_2-$[Cu_2I_2\mathbf{L}_2]_n$ before and after reduction experiment were performed to confirm catalyst stability of polymeric $[Cu_2I_2\mathbf{L}_2]_n$ shell (Figs. S3, S5).

3.4. Proposed mechanism

In the current study, polymeric cluster $[Cu_2I_2\mathbf{L}_2]_n$ was constructed *in situ* on the surface of TiO_2, the resulting core-shell TiO_2-$[Cu_2I_2\mathbf{L}_2]_n$ nanocomposite shows an effective optical response in the visible-light region. The proposed mechanism is illustrated in Fig. 6. When copper(I) centers are excited under visible-light illumination [61], photogenerated electrons transfer from the excited state $[Cu_2I_2\mathbf{L}_2]_n$ into the conduction band of TiO_2, and then be captured by Cr(VI) ions, resulting in the reduction of Cr(VI) to Cr(III) [4]. Combining the crystal structure information, we can find that, the polymeric cluster structure, the face-to-face π-π stacking interaction of anthrancenes in $[Cu_2I_2\mathbf{L}_2]_n$ and charge-transfer complex formed through anthracene and TiO_2 all promote intramolecular/intermolecular electrons transfer.

The success of the current *in situ* strategy to construct efficient visible-light photoactive system, resulting from (i) the high affinity of polycyclic unit in sensitizer on the surface of TiO_2, which anchors **L** on the TiO_2 surface and construct effective electron transfer path to TiO_2, (ii) the high reactivity of copper(I) and soft Se to bring an easy synthesis of stable sensitizer, (iii) polymeric cluster shell to improve the stability of CT complex and efficiency of the electron transfer, and (iv) high optical-active copper(I) cluster center, combining the effective electron donors Se and I, which leads to energetically favorable electron transfer from excited state of sensitizer to the conduction band edge of TiO_2.

4. Conclusion

Herein, we report a new *in situ* surface assembly strategy for the preparation of polymeric copper(I) iodine cluster sensitized TiO_2, core-shell TiO_2-$[Cu_2I_2\mathbf{L}_2]_n$ nanocomposites, based upon selenoanthracene ligand and CuI. It showed efficient photocatalytic activity to aqueous Cr(VI) reduction under visible-light (λ > 400 nm), with good chemical stability and long term activity. Studies show that selenoether based polymeric Cu_2I_2 cluster and the high affinity of anthrancene unit on the surface of TiO_2 endow the efficiency of the whole photoactive system, as well as high stability. Overall, our work provides new insights into the fabrication of visible-light photoactive TiO_2-based nanocomposites with low-cost copper complexes. Further studies in constructing selenoether based polymeric copper(I) clusters and tuning the potential levels by structural constraints will be conducted in the future.

Acknowledgements

We gratefully acknowledge financial support from the National Basic Research Program of China (973 Program) (No. 2013CB733504), National Natural Science Foundation (Grant Nos. 21171092 and 21671101) and NanjingTech Research Foundation for Dr. Wei Ji.

Appendix A. Supplementary data

Supplementary data associated with this article can be found, in the online version, at http://dx.doi.org/10.1016/j.apcatb.2016.12.041.

References

[1] J.G. Wang, X.R. Li, X. Li, J. Zhu, H.X. Li, Nanoscale 5 (2013) 1876.
[2] A. Tanaka, K. Nakanishi, R. Hamada, K. Hashimoto, H. Kominami, ACS Catal. 3 (2013) 1886–1891.
[3] K. Fujiwara, Y. Deligiannakis, C.G. Skoutelis, S.E. Pratsinis, Appl. Catal. B: Environ. 154–155 (2014) 9–15.
[4] Q. Cheng, C.W. Wang, K. Doudrick, C.K. Chan, Appl. Catal. B: Environ. 176–177 (2015) 740–748.
[5] Y.Q. Qu, X.F. Duan, Chem. Soc. Rev. 42 (2013) 2568–2580.

[6] J. Lim, D. Monllor-Satoca, J.S. Jang, S. Lee, W. Choi, Appl. Catal. B: Environ. 152–153 (2014) 233–240.
[7] N. Nishiyama, Y. Fujiwara, K. Adachi, K. Inumaru, S. Yamazaki, Appl. Catal. B: Environ. 176–177 (2015) 347–353.
[8] P. Zhang, M. Fujitsuka, T. Majima, Appl. Catal. B: Environ. 185 (2016) 181–188.
[9] H. Imahori, T. Umeyama, S. ITO, Accounts Chem. Res. 42 (2009) 1809–1818.
[10] C.C. Chen, W.H. Ma, J.C. Zhao, Chem. Soc. Rev. 39 (2010) 4206–4219.
[11] T. Kamegawa, S. Matsuura, H. Seto, H. Yamashita, Angew. Chem. Int. Ed. 52 (2013) 916–919.
[12] H. Park, H.I. Kim, G.H. Moon, W. Choi, Energy Environ. Sci. 9 (2016) 411–433.
[13] G.C. Vougioukalakis, A.I. Philippopoulos, T. Stergiopoulos, P. Falaras, Coordin. Chem. Rev. 255 (2011) 2602–2621.
[14] N. Alonso-Vante, J.F. Nierengartenb, J.P. Sauvage, J. Chem. Soc. Dalton Trans. (1994) 1649–1654.
[15] N. Armaroli, Chem. Soc. Rev. 30 (2001) 113–124.
[16] C.L. Linfoot, P. Richardson, T.E. Hewat, O. Moudam, M.M. Forde, A. Collins, F. White, N. Robertson, Dalton Trans. 39 (2010) 8945–8956.
[17] J. Huang, O. Buyukcakir, M.W. Mara, A. Coskun, N.M. Dimitrijevic, G. Barin, O. Kokhan, A.B. Stickrath, R. Ruppert, D.M. Tiede, J.F. Stoddart, J.P. Sauvage, L.X. Chen, Angew. Chem. Int. Ed. 51 (2012) 12711–12715.
[18] M. Sandroni, L. Favereau, A. Planchat, H. Akdas-Kilig, N. Szuwarski, Y. Pellegrin, E. Blart, H. Le Bozec, M. Boujtita, F. Odobel, J. Mater. Chem. A 2 (2014) 9944–9947.
[19] M.W. Mara, D.N. Bowman, O. Buyukcakir, M.L. Shelby, K. Haldrup, J. Huang, M.R. Harpham, A.B. Stickrath, X. Zhang, J.F. Stoddart, A. Coskun, E. Jakubikova, L.X. Chen, J. Am. Chem. Soc. 137 (2015) 9670–9684.
[20] C.E. Housecroft, E.C. Constable, Chem. Soc. Rev. 44 (2015) 8386–8398.
[21] M. Magni, P. Biagini, A. Colombo, C. Dragonetti, D. Roberto, A. Valore, Coord. Chem. Rev. 322 (2016) 69–93.
[22] M.W. Mara, K.A. Fransted, L.X. Chen, Coord. Chem. Rev. 282 (2015) 2–18.
[23] T. Bessho, E.C. Constable, M. Graetzel, A. Hernandez Redondo, C.E. Housecroft, W. Kylberg, M.K. Nazeeruddin, M. Neuburger, S. Schaffner, Chem. Commun. 32 (2008) 3717–3719.
[24] S. Keller, E.C. Constable, C.E. Housecroft, M. Neuburger, A. Prescimone, G. Longo, A. Pertegas, M. Sessolo, H.J. Bolink, Dalton Trans. 43 (2014) 16593–16596.
[25] E. Schönhofer, B. Bozic-Weber, C.J. Martin, E.C. Constable, C.E. Housecroft, J.A. Zampese, Dyes Pigm. 115 (2015) 154–165.
[26] S.O. Fürer, L.Y.N. Luu, B. Bozic-Weber, E.C. Constable, C.E. Housecroft, Dyes Pigm. 132 (2016) 72–78.
[27] S. Perruchas, X.F. Le Goff, S. Maron, I. Maurin, F. Guillen, A. Garcia, T. Gacoin, J.P. Boilot, J. Am. Chem. Soc. 132 (2010) 10967–10969.
[28] Q. Benito, X.F. Le Goff, S. Maron, A. Fargues, A. Garcia, C. Martineau, F. Taulelle, S. Kahlal, T. Gacoin, J.P. Boilot, S. Perruchas, J. Am. Chem. Soc. 136 (2014) 11311–11320.
[29] Q. Benito, I. Maurin, T. Cheisson, G. Nocton, A. Fargues, A. Garcia, C. Martineau, T. Gacoin, J.P. Boilot, S. Perruchas, Chem. Eur. J. 21 (2015) 5892–5897.
[30] D. Volz, Y. Chen, M. Wallesch, R. Liu, C. Flechon, D.M. Zink, J. Friedrichs, H. Flugge, R. Steininger, J. Gottlicher, C. Heske, L. Weinhardt, S. Brase, F. So, T. Baumann, Adv. Mater. 27 (2015) 2538–2543.
[31] Y. Yu, X.M. Zhang, J.P. Ma, Q.K. Liu, P. Wang, Y.B. Dong, Chem. Commun. 50 (2014) 1444–1446.
[32] S. Cho, Y. Jeon, S. Lee, J. Kim, T.H. Kim, Chem. Eur. J. 21 (2015) 1439–1443.
[33] W. Ji, J. Qu, S. Jing, D.R. Zhu, W. Huang, Dalton Trans. 45 (2016) 1016–1024.
[34] Y.L. Hou, R.W.Y. Sun, X.P. Zhou, J.H. Wang, D. Li, Chem. Commun. 50 (2014) 2295–2297.
[35] Y.L. Hou, S.X. Li, R.W.Y. Sun, X.Y. Liu, S.W. Ng, D. Li, Dalton Trans. 44 (2015) 17360–17365.
[36] Q. Xiang, J.G. Yu, M. Jaroniec, Chem. Soc. Rev. 41 (2012) 782–796.
[37] J.S. Lee, K.H. You, C.B. Park, Adv. Mater. 24 (2012) 1084–1088.
[38] J. Zhang, Z.P. Zhu, Y.P. Tang, X.L. Feng, J. Mater. Chem. A 1 (2013) 3752–3756.
[39] Z.X. Gan, X.L. Wu, M. Meng, X.B. Zhu, L. Yang, P.K. Chu, ACS Nano 8 (2014) 9304–9310.
[40] Y.Q. Liu, W. Ji, H.Y. Zhou, Y. Li, S. Jing, D.R. Zhu, J. Zhang, RSC Adv. 5 (2015) 42689–42697.
[41] Y.S. Seo, C. Lee, K.H. Lee, K.B. Yoon, Angew. Chem. Int. Ed. 44 (2005) 910–913.
[42] A. Ramakrishnan, S. Neubert, B. Mei, J. Strunk, L. Wang, M. Bledowski, M. Muhler, R. Beranek, Chem. Commun. 48 (2012) 8556–8558.
[43] T.E. Hewat, L.J. Yellowlees, N. Robertson, Dalton Trans. 43 (2014) 4127–4136.
[44] G.M. Sheldrick, Acta crystallogr, Sect. C: Cryst. Struct. Commun. 71 (2015) 3.
[45] C. Janiak, J. Chem. Soc. Dalton Trans. (2000) 3885–3896.
[46] M.H. Yoon, A. Facchetti, C.E. Stern, T.J. Marks, J. Am. Chem. Soc. 128 (2006) 5792–5801.
[47] Y.F. Li, A.Y. Pang, C.J. Wang, M.D. Wei, J. Mater. Chem. 21 (2011) 17259–17264.
[48] G. Kim, S.H. Lee, W. Choi, Appl. Catal. B: Environ. 162 (2015) 463–469.
[49] W.A. Maza, A.J. Haring, S.R. Ahrenholtz, C.C. Epley, S.Y. Lin, A.J. Morris, Chem. Sci. 7 (2016) 719–727.
[50] W.D. Shi, J.Q. Shi, S. Yu, P. Liu, Appl. Catal. B: Environ. 138–139 (2013) 184–190.
[51] D. Praveen Kumar, N. Lakshmana Reddy, B. Srinivas, V. Durgakumari, V. Roddatis, O. Bondarchuk, M. Karthik, Y. Ikuma, M.V. Shankar, Sol. Energ. Mat. Sol. C 146 (2016) 63–71.
[52] Y.J. Zhu, N. Olson, J. Thomas, P. Beebe, Environ. Sci. Technol. 35 (2001) 3113–3121.
[53] D.Q. Yang, J.F. Rochette, E. Sacher, J. Phys. Chem. B 109 (2005) 4481–4484.
[54] D.Q. Yang, B. Hennequin, E. Sacher, Chem. Mater. 18 (2006) 5033–5038.
[55] L.C. Liu, Z. Liu, A.N. Liu, X.R. Gu, C.Y. Ge, F. Gao, L. Dong, ChemSusChem 7 (2014) 618–626.
[56] M.S. Kahouech, K. Hriz, S. Touaiti, J. Bassem, Mate. Res. Bull. 75 (2016) 144–154.
[57] J.B. Cai, X.Q. Wu, S.X. Li, F.Y. Zheng, ACS Sustain. Chem. Eng. 4 (2016) 1581–1590.
[58] A. Hagfeldt, G. Boschloo, L. Sun, L. Kloo, H. Pettersson, Chem. Rev. 110 (2010) 6595–6663.
[59] M.D. Zhang, Z.Y. Zhang, Z.Q. Bao, Z.M. Ju, X.Y. Wang, H.G. Zheng, J. Ma, X.F. Zhou, J. Mater. Chem. A 2 (2014) 14883–14889.
[60] Y.C. Chen, H.H. Chou, M.C. Tsai, S.Y. Chen, J.T. Lin, C.F. Yao, K. Chen, Chem. Eur. J. 18 (2012) 5430–5437.